

ON APPROXIMATION OF ORIENTATION DISTRIBUTIONS BY MEANS OF SPHERICAL RIDGELETS

Oleg V. Michailovich*

University of Waterloo
Dept. of Electrical and Computer Engineering
Waterloo, ON, Canada

Yogesh Rathi

Harvard Medical School
Brigham and Women's Hospital
Boston, MA, USA

ABSTRACT

Visualization and analysis of the micro-architecture of brain parenchyma by means of magnetic resonance imaging (MRI) is currently considered to be one of the most powerful methods for interrogating cerebral tissue. Unfortunately, the diffusion tensor imaging (DTI) which is standardly used for estimating the local orientations of brain fibers, is prone to substantial estimation errors whenever a voxel of interest contains more than one fiber. In such a case, a much more accurate analysis is possible using the high angular resolution diffusion imaging (HARDI) that represents local diffusion by its apparent coefficients measured as a function of orientations. In this note, a novel approach to enhancing and modeling the HARDI signals using multiresolution bases of spherical ridgelets is presented. In addition to its desirable properties of being adaptive, sparsifying, and efficiently computable, the proposed modeling leads to analytical computation of the orientation distribution functions associated with the measured diffusion, thereby providing a fast and robust analytical solution for q-ball imaging.

Index Terms— Q-ball imaging, orientation distribution function, spherical harmonics, ridgelets, and MR-DTI

1. INTRODUCTION

The need for development of more accurate diagnostic tools for predicting and monitoring cerebral and neurological diseases necessitate the invention of novel methods for imaging the structure of brain tissue along with physiological parameters of its parenchyma. In magnetic resonance imaging, diffusion tensor imaging (DTI) [1] offers the possibility of acquiring a multitude of exquisite details on the microstructure of brain tissue via measuring the diffusion of water molecules across the cerebral fibers. The most advanced application of DTI is certainly that of fiber tracking in the brain, which, in combination with functional MRI, seems to be opening a window on the important issue of connectivity [2].

*This research was supported by a discovery grant from NSERC - the Natural Sciences and Engineering Research Council of Canada.

Unfortunately, the classical DTI has a fundamental limitation which stems from the fact that it assumes each image voxel to be occupied by *a single* fiber. Consequently, the diffusion measurements at the sites when the fibers (or bundles thereof) cross, touch upon each other, or diverge can be rather inaccurate. To overcome this deficiency of DTI, *high angular resolution diffusion imaging* (HARDI) was proposed in [3], where the diffusion is measured directly via sampling the MR signal over a spherical shell in diffusion wavevector space.

Despite of its numerous advantages, until recently, the extensive use of HARDI has been hampered by the absence of computationally efficient tools necessary to derive the *orientation distribution functions* (ODF) corresponding to HARDI signals. To resolve this problem, Tuch *et al.* [4] have introduced the *q-ball imaging* method, in which the ODFs are estimated by applying the Funk-Radon transform to numerically interpolated HARDI data. However, the property of this method of being prone to both interpolation and measurement errors necessitated further research in this direction. As a result, the applicability of spherical Fourier analysis to q-ball imaging was recently demonstrated in [5, 6], where ODFs are recovered by approximating the HARDI data by finite series of spherical harmonics, followed by analytically computing the ODFs by virtue of the Funk-Hecke formula. A regularized version of the above approach was recently proposed in [7] as well.

Unfortunately, the most valuable property of the above-mentioned Fourier methods of being *analytical* seems to be counterbalanced by the fact that accurately approximating the ODFs may require a relatively large number of spherical harmonics to be used per one voxel. Needless to say that this fact could represent a real problem in the situations, where the Fourier coefficients representing the ODFs need to be further used for, e.g., signal interpolation, segmentation, etc. Storing a relatively large number of representation coefficients may be another issue that is likely to arise in this case as well.

The main goal of the present note is to introduce a different basis of functions using which one can *analytically* represent the ODF using a relatively small number of representation coefficients. Particularly, we introduce and develop the

concept of *spherical ridgelets* following the conceptual lines defined in [8]. It is also shown how the ridgelet approximations can be used for recovering the ODFs using only about half an order of magnitude fewer representation coefficients as compared to the case of spherical harmonics.

Finally, it should be noted that the proposed ridgelet analysis is different from the one recently presented in [9], where a “flat” ridgelet transform is applied to localized regions of the unit sphere. Moreover, our construction is neither similar to that in [10], where a ridgelet-like transformation is derived using the theory Riesz potentials. Thus, to the best of our knowledge, the proposed ridgelet analysis as well as its use for analytically approximating the ODFs is reported in this paper for the first time.

2. DIFFUSION FUNCTION AND ODF

In DTI, the *diffusion function* $p(\mathbf{r})$ defines the ensemble-averaged probability for a spin to undergo a relative displacement $\mathbf{r} \in \mathbb{R}^3$ in the experimental diffusion time τ . The orientation structure of such a diffusion function is commonly described using the diffusion *orientation distribution function* (ODF) $\psi(\mathbf{u})$ which is defined as

$$\psi(\mathbf{u}) = \frac{1}{Z} \int_0^\infty p(\alpha \mathbf{u}) d\alpha, \quad (1)$$

with \mathbf{u} being a direction on the *unit sphere* Ω , and Z standing for a normalization constant.

The basis of q-ball imaging is formed by the fact that the ODF $\psi(\mathbf{u})$ can be closely approximated by the Funk-Radon transform \mathcal{R} of the raw HARDI signal evaluated on the unit sphere Ω in the q -space, *viz.* [4]

$$\psi(\mathbf{u}) \simeq \mathcal{R}[S(\mathbf{q})] = \int_\Omega \delta(\mathbf{u} \cdot \mathbf{q}) S(\mathbf{q}) d\eta(\mathbf{q}), \quad (2)$$

where $S(\mathbf{q})$ is the HARDI signal, δ is the delta function, the dot denotes the standard inner product in \mathbb{R}^3 , and $\eta(\mathbf{q})$ is the surface element.

Under some fairly general assumptions, the diffusion signal $S(\mathbf{q})$ which originates from a voxel containing M fibers, can be modeled as [7]

$$S(\mathbf{q}) = S_0 \sum_{k=1}^M p_k \exp\{-b(\mathbf{q}^T \mathbf{D}_k \mathbf{q})\} + n(\mathbf{q}), \quad (3)$$

where S_0 is a constant scaling factor, \mathbf{D}_k is a 3×3 diffusion tensor associated the k -th fiber, $b > 0$ is a scanner dependent constant, $n(\mathbf{q})$ accounts for both measurement and model noises, and $\{p_k\}$ are proportionality constants obeying $\sum_{k=1}^M p_k = 1$. Ignoring for the moment the noise in (3), it is straightforward to show that the ODF corresponding to the $S(\mathbf{q})$ in (3) is given by [7]

$$\psi(\mathbf{u}) = \sum_{k=1}^M \frac{p_k}{Z} \sqrt{\frac{\pi b}{\mathbf{u}^T \mathbf{D}_k \mathbf{u}}}. \quad (4)$$

3. REPRESENTATION OF SPHERICAL FUNCTIONS

It is well known that any square-integrable function defined on the unit square Ω can be represented by a Fourier series expansion, *viz.* as a linear combination of spherical harmonics. It is worthwhile noting that the spherical harmonics $Y_{j,n}$ of degree n (with $j = 1, 2, \dots, 2n + 1$) are defined as the eigenfunctions of the Beltrami operator Δ^* on Ω with respect to the eigenvalue $-n(n + 1)$. Moreover, it is straightforward to show that the dimension of the “truncated space” $\text{Harm}_{0,\dots,m} = \oplus_{n=0}^m \text{span}\{Y_{j,n}\}_{j=1}^{2n+1}$ is equal to $(m + 1)^2$.

Similar to the case of Fourier exponentials over \mathbb{R}^d , the spherical harmonics $\{Y_{j,n}\}$ have poor localization properties, being supported over all Ω . Thus, in the case when a function of interest contains locally supported details, a more informative analysis is possible by replacing the spherical harmonics by functions with compact support. One way to construct such a localized basis is by using the kernel function of the form [11]

$$K(\mathbf{u}, \mathbf{v}) = K(\mathbf{u} \cdot \mathbf{v}) = \sum_{n=0}^{\infty} A_n^{-2} \frac{2n+1}{4\pi} P_n(\mathbf{u} \cdot \mathbf{v}), \quad (5)$$

where $P_n : [-1, 1] \rightarrow \mathbb{R}$ is the Legendre polynomial of degree n , and the sequence $\{A_n\}$ is required to satisfy the summability condition $\sum_{n=0}^{\infty} A_n^{-2} \frac{2n+1}{4\pi} < \infty$. It can then be rigorously proven [11] that, given a countable dense set of points $\{u_1, u_2, \dots\}$ on the sphere Ω , the closure of $\text{span}_{n=0,1,\dots} K(u_n, \cdot)$ is dense in $L^2(\Omega)$ provided $A_n \neq 0$ for all n .

Although there exists a variety of different definitions of $K(\mathbf{u}, \mathbf{v})$, for the sake of concreteness as well as due to its exceptional localization properties in both spatial and frequency domains, in what follows we use the Gauss-Weierstrass kernel which is defined by

$$A_n = A_n^\rho = \exp\{-\rho n(n + 1)\}, \quad \rho > 0, \quad (6)$$

This kernel is depicted in Subplot A of Fig. 1 as a function of $\cos(\theta)$ (with $-\pi \leq \theta \leq \pi$), while Subplot B of the figure shows $K(\mathbf{u}_0, \mathbf{v})$ for a *fixed* \mathbf{u}_0 and $\mathbf{v} \in \Omega$. (Note that, in Fig. 1, larger values of the kernel are represented by reddish colors, while blue corresponds to zero).

4. SPHERICAL RIDGELETS

The smoothness properties of the Gauss-Weierstrass (GW) kernel can be controlled via changing the value of $\rho > 0$ in (6). Specifically, when $\rho \rightarrow 0$, the kernel converges to a delta function, whereas when ρ goes to infinity, the kernel’s energy becomes uniformly distributed over Ω . This fact suggests the possibility of a multiresolution analysis over Ω with $K(\mathbf{u}, \mathbf{v})$ used as a generating function [11]. However, before applying such an analysis to the problem at hand, it is instructive to

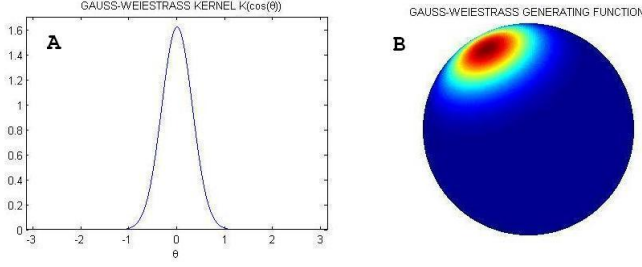


Fig. 1. (Subplot A) The Gauss-Weierstrass kernel as a function of $\cos(\theta)$; (Subplot B) The same kernel $K(\mathbf{u}, \mathbf{v})$ shown on the unit sphere for a fixed value of \mathbf{u} .

take a closer look into the similarity between the GW-kernel and HARDI signals.

The model (3) suggests that a (noise-free) HARDI signal is formed as a linear combination of several isotropic diffusion signals. An example of such an isotropic signal is shown in Subplot A of Fig. 2, where its amplitude is visualized in the polar coordinate system as a function of orientation. The ODF corresponding to this signal is shown in Subplot B of the same figure, where it indicates the orientation of the diffusion flow. One can see that, as opposed to the GW-kernel, the support of the HARDI signal is not compact, being “smeared” all over the *great circle* perpendicular to the direction of diffusion. Thus, it is reasonable to conclude that representing the HARDI signal by a linear combination of scaled and shifted versions of the GW-kernel will require a relatively large number of representation coefficients.

A sparser representation of HARDI signals is possible by a different kind of analysis which can be designed as follows. First, let a *ridgelet generating function* Φ_ρ to be defined as

$$\begin{aligned} \Phi_\rho(\mathbf{u}, \mathbf{v}) &= \frac{1}{2\pi} \int_{\Omega} \delta(\mathbf{u} \cdot \mathbf{p}) K(\mathbf{p} \cdot \mathbf{v}) \eta(\mathbf{p}) = \\ &= \sum_{n=0}^{\infty} c_n^\rho \frac{2n+1}{4\pi} P_n(\mathbf{u} \cdot \mathbf{v}), \end{aligned} \quad (7)$$

where $c_n^\rho = e^{-\rho(n(n+1))} \sqrt{\frac{(-1)^n}{\pi} \frac{\Gamma((n+1)/2)}{\Gamma((n+2)/2)}}$ (with Γ being the gamma function) if n is even, and $c_n^\rho = 0$ when n is odd. Subsequently, it is straightforward to show that the Funk-Radon transform Ψ_ρ of Φ_ρ is given by

$$\Psi_\rho(\mathbf{u}, \mathbf{v}) = \mathcal{R}[\Phi_\rho] = \sum_{n=0}^{\infty} b_n^\rho \frac{2n+1}{4\pi} P_n(\mathbf{u} \cdot \mathbf{v}), \quad (8)$$

with

$$b_n^\rho = \begin{cases} 2 e^{-\rho(n(n+1))} \left[\frac{\Gamma((n+1)/2)}{\Gamma((n+2)/2)} \right]^2, & \text{if } n \text{ is even} \\ 0, & \text{if } n \text{ is odd} \end{cases} \quad (9)$$

The functions Φ_ρ and Ψ_ρ are shown in Subplots C and D of Fig. 2, respectively, for $\rho = 0.06$. One can see that, similarly to the HARDI signal shown in Subplot A, the energy of

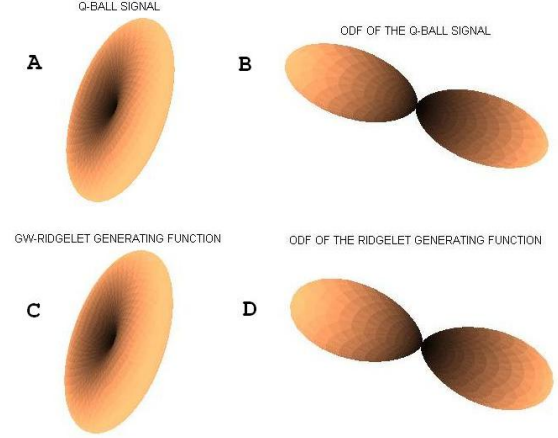


Fig. 2. Subplot(A) Single-filter HARDI signal $S(\mathbf{q})$; (Subplot B) The ODF corresponding to $S(\mathbf{q})$; Subplot (C) A Gauss-Weierstrass ridgelet generating function (RGF); Subplot(D) The Funk-Radon transform of the RDF.

Φ_ρ is concentrated around a great circle (much like the energy of “planar” ridgelets is concentrated along straight projection paths across the plane). Moreover, the shape of Ψ_ρ appears to be in a good agreement with the shape of signal’s ODF.

The above considerations suggest that HARDI signals can be efficiently represented by a multiresolution analysis generated by Φ_ρ . Specifically, we define a *spherical ridgelet* X_j to be the difference between two differently scaled ridgelet generating functions, namely

$$X_j(\mathbf{u}, \mathbf{v}) = \Phi_{\rho 4^{-(j+1)}}(\mathbf{u}, \mathbf{v}) - \Phi_{\rho 4^{-j}}(\mathbf{u}, \mathbf{v}), \quad (10)$$

with $j = 0, 1, \dots$. Subsequently, at the direction defined by a given \mathbf{u}_i and at resolution j , the ridgelet coefficient $s_{i,j}$ of signal $S(\mathbf{q})$ is computed as

$$s_{i,j} = \langle S, X_j(\mathbf{u}_i, \cdot) \rangle = \int_{\Omega} S(\mathbf{q}) X_j(\mathbf{u}_i, \mathbf{q}) \eta(\mathbf{q}). \quad (11)$$

It should be noted that the above inner products can be computed in a closed form manner, using the formula given, e.g., by Eq.2 in [9].

Finally, we note that, in practice, HARDI signals are represented by a finite number of sampling directions $\{\mathbf{u}_i\}_{i=1}^N$. (Thus, for example, in the case of icosahedron tessellation of second order, $N = 162$.) In this case, the spherical ridgelets can be defined for all *non-collinear* directions $\{\tilde{\mathbf{u}}_i\}$, resulting in the following set of functions

$$\{\Phi_\rho(\tilde{\mathbf{u}}_i, \cdot), \{X_j(\tilde{\mathbf{u}}_i, \cdot)\}_{j=0,1,\dots}\}, i = 1, 2, \dots \quad (12)$$

The above set is generally overcomplete. The overcompleteness, however, suggests the possibility of sparse analysis, in which case the data signals are represented by as few regressors as possible. In the current work, in order to find such representations, the *orthogonal matching pursuit* method of [12]

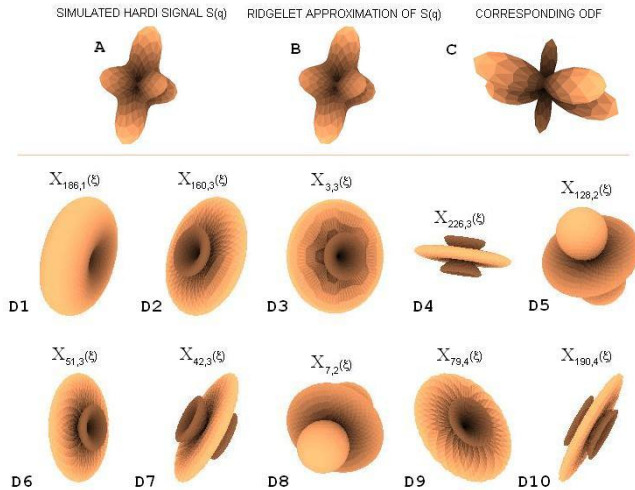


Fig. 3. (Subplot A) Simulated triple-fiber HARDI signal; (Subplot B) Ridgelet approximation of the signal; (Subplot C) The corresponding ODF; (Subplots D1-D10) The approximating ridgelets.

Table 1. MSE (in %) of estimating the triple-fiber ODFs.

| SNR = | 20 dB | 15 dB | 10 dB |
|---------------------|-------|-------|-------|
| Spherical harmonics | 4.1 | 4.3 | 5.2 |
| Spherical ridgelets | 3.5 | 3.9 | 4.8 |

was employed due to its exceptional computational efficiency. An example of the proposed method is demonstrated in Fig. 3, Subplots A, B, and C of which show a HARDI signal simulated according to (3), its ridgelet approximation, and the corresponding ODF, respectively. Subplots D1-D10 of the figure show the 10 spherical ridgelets used for the representation.

5. SIMULATION RESULTS

In the experimental part of this paper, we compare both the accuracy and complexity of estimating the ODFs by means of Fourier and ridgelet analysis. In order to perform the comparison in a quantitative manner, simulated data sets produced as detailed in [7] were used. The maximal order of spherical harmonics was set to be equal to 8. Note that, since HARDI signals are symmetric, only even-order harmonics need to be used in this case, resulting in the total of 45 Fourier coefficients per signal. At the same time, the maximal number of spherical ridgelets was set to be equal to 10.

Table 1 shows the normalized mean squared errors (computed based on the results of 200 independent trials) of estimating the simulated ODFs using the spherical harmonics and spherical ridgelets. One can see that, despite the considerable difference in the number of representation coefficients used in these cases, the ridgelet analysis provides more accu-

rate estimation results for all tested SNRs. This fact supports the viability of the proposed ridgelet analysis as an efficient and accurate tool for analytic q-ball imaging.

6. REFERENCES

- [1] D. Le Bihan, E. Breton, D. Lallemand, and et al., “MR imaging of intravoxel incoherent motions: Application to diffusion and perfusion in neurological disorders,” *Radiology*, vol. 161, pp. 401–407, 1985.
- [2] P. J. Basser, S. Pajevic, C. Pierpaoli, J. Duda, and A. Aldroubi, “In vivo fiber tractography using DT-MRI data,” *Magn. Reson. Med.*, vol. 44, pp. 625–632, 2000.
- [3] D. S. Tuch, T. G. Reese, M. R. Wiegell, and V. J. Wedeen, “Diffusion MRI of complex neural architecture,” *Neuron*, vol. 40, pp. 885–895, 2003.
- [4] D. S. Tuch, “Q-ball imaging,” *Magn. Reson. Med.*, vol. 52, pp. 1358–1372, 2004.
- [5] A. W. Anderson, “Measurement of fiber orientation distributions using high angular resolution diffusion imaging,” *Magn. Reson. Med.*, vol. 54, pp. 1194–1206, 2005.
- [6] C. P. Hess, P. Mukherjee, E. T. Han, D. Xu, and D. R. Vigneron, “Q-ball reconstruction of multimodal fiber orientations using the spherical harmonic basis,” *Magn. Reson. Med.*, vol. 56, pp. 104–117, 2006.
- [7] M. Descoteaux, E. Angelino, S. Fitzgibbons, and R. Deriche, “A linear and regularized ODF estimation algorithm to recover fibers in Q-ball imaging,” Tech. Rep. RR-5768, Institut National de Recherche en Informatique et en Automatique, Nov. 2005.
- [8] E. J. Candes and D. L. Donoho, “Ridgelets: a key to high-dimensional intermittency?,” *Phil. Trans. R. Soc. Lond.*, vol. 357, pp. 2495–2509, 1999.
- [9] J.-L. Starck, Y. Moudden, P. Abrial, and M. Nguyen, “Wavelets, ridgelets and curvelets on the sphere,” *Astron. Astrophys.*, vol. 446, pp. 1191–1204, 2006.
- [10] B. Rubin, “Spherical Radon transform and related wavelet transforms,” *Appl. Comput. Harm. Anal.*, vol. 5, pp. 202–215, 1998.
- [11] W. Freeden and F. Schreiner, “Orthogonal and non-orthogonal multiresolution analysis, scale discrete and exact fully discrete wavelet transform on the sphere,” *Constr. Approx.*, vol. 14, pp. 493–515, 1998.
- [12] Y. Pati, R. Rezaifar, and P. Krishnaprasad, “Orthogonal matching pursuit: recursive function approximation with applications to wavelet decomposition,” in *Proc. the 27th Annual Asilomar Conference on Signals, Systems, and Computers*, Nov. 1993.